JOURNAL OF Materials CHEMISTRY

Self propagating high temperature synthesis of $BaFe_{12-x}Cr_xO_{19}$ and $Li_{0.5}Fe_{2.5-x}Cr_xO_4$†

Ivan P. Parkin,[a] Maxim V. Kuznetsov[b] and Quentin A. Pankhurst[b]

[a]*Department of Chemistry, University College London, 20 Gordon Street, London, UK WC1H 0AJ*
[b]*Department of Physics and Astronomy, University College London, Gower Street, London, UK WC1E 6BT*

Received 20th March 1998, Accepted 26th May 1998

Thermal initiation of a mix of BaO_2, Fe_2O_3, Cr_2O_3 and iron powder in air induces a self propagating reaction with velocity 1–2 mm s^{-1} and the formation of predominantly $BaFe_{12-x}Cr_xO_{19}$. Thermal initiation of a mixture of Li_2O_2, Fe_2O_3, Cr_2O_3 and iron powder in air also induces a propagation wave with formation of predominantly $Li_{0.5}Fe_{2.5-x}Cr_xO_4$. Heating either product mixture to 1150–1200 °C for 2 h produces phase pure crystalline powders of $BaFe_{12-x}Cr_xO_{19}$ and $Li_{0.5}Fe_{2.5-x}Cr_xO_4$. An external 1.1 T magnetic field increased the SHS synthesis wave velocity and temperature for both hard ($BaFe_{12-x}Cr_xO_{19}$) and soft ferrites ($Li_{0.5}Fe_{2.5-x}Cr_xO_4$). Materials synthesised in a magnetic field showed significant changes in H_c, σ_{max} and σ_r compared to those synthesized in zero field. All the samples were characterised by X-ray powder diffraction, FTIR, VSM, EDAX/SEM and Mössbauer spectroscopy.

Conventional synthesis of inorganic ceramic materials invariably involves multiple grinding, heating and cooling cycles of suitable precursors.[1] Reactions usually require extensive time periods primarily because interdiffusion of reacting solids is slow even at high temperatures.[2] Many techniques have been developed to surmount the solid state diffusion barrier including precipitation synthesis,[3] the sol–gel process,[4] hydrothermal synthesis,[5] melt formation and formation of suitable precursors which have inbuilt molecular triggers or thermal 'Achilles Heels'.[6] These processes aim to reduce the diffusion path length of the reacting components often by mixing the required elements on the atomic scale. They all have a common link in that external heating is required to promote the reaction. These processes are extremely successful, each technique having merits for certain applications. Two relatively new synthetic variants have been developed which negate the need to externally heat a reaction, these are based on self propagating reactions which provide the energy to overcome the solid state diffusion barrier internally, within the starting materials, by promoting an exothermic chemical reaction. These processes are termed self propagating high temperature synthesis (SHS)[7] and solid state metathesis reactions (SSM).[8,9]

The field of SHS reactions was pioneered over twenty-five years ago by the work of Merzanhov and co-workers of the Institute of Structural Macrokinetics in Chernogolovka.[10] Today over fifteen countries are involved in SHS synthesis producing in excess of three hundred papers a year.[10] Self-propagating reactions are not a new phenomenon. The thermite reaction which is used to join railway tracks and in welding [eqn. (1)] and the Goldsmidt reaction [eqn. (2)] have been known for over a hundred years.[11] The reactions are extremely exothermic and produce temperatures up to 3000 °C. SHS processes are used commercially, for example, the Goldsmidt reaction is used by London and Scandinavia Metallurgical Co to produce one third of the worlds chromium metal supply.

$$Fe_2O_3 + Al \rightarrow Fe + Al_2O_3 \quad (1)$$

$$Cr_2O_3 + Al \rightarrow Cr + Al_2O_3 \quad (2)$$

†Basis of the presentation given at Materials Chemistry Discussion No. 1, 24–26 September 1998, ICMCB, University of Bordeaux, France.

SHS reactions are also able to make complex intermetallic compounds, metal nitrides, oxides, borides and carbides.[12–14] The reactions can be promoted in a mold and extrusion technologies can be used to manipulate the molten reaction zone to produce complex net shape products such as automotive catalytic converters.[15] Other applications of the SHS reaction include its use in sealing up toxic and radioactive materials by forming a glass and centripetal SHS reactions which have been used to coat the inner surfaces of pipes.[16] Despite these advances SHS reactions have not found widespread applicability in commercial synthesis especially of structural materials where the establishment of fully dense ceramics is difficult unless the SHS process is accompanied by simultaneous densification.[17]

In contrast to SHS reaction solid state metathesis reactions have only been developed (primarily by Kaner *et al.*[18] and Parkin *et al.*[19]) over the last six years. The reactions tend to be less exothermic than SHS processes and because a salt is co-produced in the reaction this can act as an inbuilt heat break that limits the reaction temperature to the boiling point of the salt [eqn. (3)]. Thus SSM reaction can produce ceramic materials that are relatively thermally sensitive. Both SSM and SHS reactions proceed by a propagation wave (also called synthesis wave, thermal flash or combustion wave) that moves away from the source of ignition with relatively uniform velocity, the majority of the reaction occurring in the short lived molten reaction zone. Both types of reactions are typified by rapid heating and cooling, often producing metastable products of unusual phase or composition. The thermodynamic parameters that determine reaction propagation have been worked out for both processes.[20]

$$Li_nQ + MCl_n \rightarrow MQ + nLiCl \quad (3)$$

(M = metal, Q = N, P, As, Sb, O, S, Se, Te, B)

SHS reactions have been studied under a variety of different experimental conditions. Recent experiments have included studying SHS processes in microgravity environments including drop towers and parabolic aircraft flights.[12] Other advances have included the passage of an electric current through a material during an SHS reaction. These experiments have shown profound effects including changes in product micro-

structure and elemental compositions.[21] SHS reactions can also be utilised in solution by using modified redox mixtures containing hydrazine carboxylate ligands.[22] Combustion of the solution stimulates the SHS reaction. They can also be promoted between solids and gases, liquids and gases and solids and liquids. Normally these reactions require specially developed apparatus that can withstand the extremely high pressures and temperatures generated. In the synthesis of metal oxide materials for example, it is routine to conduct the reactions under a number of atmospheres of oxygen in sealed bomb reactors.

SHS reactions are often classed as being more economical in terms of energy expenditure compared to the more conventional solid state routes. It is true that SHS reactions are faster than conventional synthesis and that they often do not require the heating costs associated with furnace heating. However, for a true energy and economic evaluation the costs and energy required to produce the starting materials as well as processing cost for both conventional and SHS have to be determined. These comparisons have been made for various classes of materials by Merzhanov.[23] He has shown that SHS is at least equivalent to and in some cases up to three times more efficient than conventional synthesis. This has lead to the establishment of manufacturing industries in Russia, Spain and Korea that exploit SHS technology.

Hexagonal ferrites ($MFe_{12-x}M'_xO_{19}$; M = Ba, Sr, Pb; M′ = Al, Cr, Ga, In, Sc, Ru[24]) are extensively utilised throughout industry for the production of permanent magnets. They are manufactured on a scale exceeding 70 000 tonnes annually.[24] We have shown previously that SHS reactions can be utilised for the formation of $SrFe_{12}O_{19}$,[25] producing materials with magnetic characteristics that are equal to commercial samples. Here, we demonstrate that SHS reactions can be utilised for the formation of both complex hard magnets $BaFe_{12-x}Cr_xO_{19}$ (x = 0, 2, 4, 6, 8) and complex soft magnets $Li_{0.5}Fe_{2.5-x}Cr_xO_4$ (x = 0, 0.75, 1.25, 1.50, 1.75). In particular we investigate the effects of carrying out an SHS reaction in an external magnetic field.

Experimental

All reagents were obtained from Aldrich Chemical Co. and used as supplied. All reagents were checked for phase and elemental purity by X-ray powder diffraction (XRD) and energy dispersive X-ray analysis (EDXA) prior to use. Manipulations, weighing and grindings were performed under a nitrogen atmosphere in a Saffron Scientific glove box. SHS reactions were carried out in air on pre-ground powders supported on a ceramic tile. Synthesis wave temperatures were obtained from $W_{0.95}Re_{0.05}$ and $W_{0.80}Re_{0.20}$ thermocouples, placed directly into the green mixtures. Samples were ground after the SHS reaction and also after sintering in a carbolite furnace at 1150–1200 °C for 2 h, heating and cooling rates were typically 20 °C min^{-1}. For the applied field SHS reactions a permanent Halbach cylinder magnet made by Magnetic Solution Limited was used. This cylinder, comprising eight NdFeB magnets, provided a horizontal field of 1.1 T transverse to the cylinder axis, with a homogeneity over a 20 mm bore cross section of better than ±0.4%. A ceramic tile or quartz tube, containing the green mixture, was placed inside a quartz tube which was in turn placed into the Halbach cylinder prior to initiation of the combustion process. Conventional samples of $BaFe_{12-x}Cr_xO_{19}$ and $Li_{0.5}Fe_{2.5-x}Cr_xO_4$ were prepared by the appropriate literature methods.[26] A commercial sample of $BaFe_{12}O_{19}$–SBF 2000 was obtained from Sakai Chemical Industries, Osaka, Japan. XRD measurements were performed on a Siemens D5000 Diffractometer in the transmission mode using germanium monochromated Cu-Kα_1 (γ = 1.5406 Å) radiation and by a Philips X-pert using Cu-Kα_1 radiation in the reflection mode. Samples were indexed using TREOR or Metrix LS programmes. Vibrating sample magnetometry was carried out on an Aerosonic 3001 magnetometer at room temperature in applied fields of up to 7.5 kOe. Scanning electron microscopy (SEM) and energy dispersive X-ray analysis EDXA were carried out with a Hitachi S-4000 instrument. Fourier transform infrared (FTIR) spectra were recorded on a Nicolet 205 instrument using pressed KBr discs. Transmission Mössbauer spectra were recorded on a Wissel MR-260 constant acceleration spectrometer. Spectra were recorded in 512 channels then numerically folded to remove baseline curvature. Calibration was performed relative to α-Fe at room temperature. Powder samples were mounted in a circular plastic cell (2 cm diameter). Data analysis was performed with the thin absorber approximation, using Lorentzian lineshapes and assuming a first order perturbation approach to the combination of electric quadrupole and magnetic hyperfine interactions. The hexagonal ferrites were fitted with a least squares fitting program, using a constrained set of at most five subspectra corresponding to the five inequivalent Fe sites in $BaFe_{12-x}Cr_xO_{19}$. The lithium ferrites $LiFe_{2.5-x}Cr_xO_4$ were fitted to the octahedral and tetrahedral environments for iron within the spinel. An additional paramagnetic/superparamagnetic iron component was fitted at high levels of chromium substitution in $LiFe_{2.5-x}Cr_xO_4$.

Preparation of $BaFe_{12-x}Cr_xO_{19}$ (x = 0, 2, 4, 6, 8)

The same general procedure was used in the synthesis for all values of x illustrated here for x = 2 (Table 1).

BaO_2 (1.196 g, 10 mmol), iron powder (2.513 g, 45 mmol),

Table 1 Molar ratios of the components used in the SHS synthesis of $BaFe_{12-x}Cr_xO_{19}$ and $Li_{0.5}Fe_{2.5-x}Cr_xO_4$. The nominal cation distribution is shown for both series; square brackets denote octahedral site occupancy, round brackets tetrahedral site occupancy and curly brackets denote five-fold coordination

$BaFe_{12-x}Cr_xO_{19}$ x	BaO_2	Fe_2O_3	Fe	Cr_2O_3	Nominal cation distribution
0	1.00	2.40	4.80	—	$Ba(Fe_2)[Fe_{6(k)}Fe_{2(f)}Fe_{1(a)}]\{Fe_1\}O_{19}$
2.0	1.00	1.60	4.80	0.80	$Ba(Fe_2)[Fe_{5(k)}Cr_{1(k)}Fe_{2(f)}Cr_{1(a)}]\{Fe_1\}O_{19}$
4.0	1.00	0.80	4.80	1.60	$Ba(Fe_2)[Fe_{3(k)}Cr_{3(k)}Fe_{2(f)}Cr_{1(a)}]\{Fe_1\}O_{19}$
6.0	1.00	—	4.80	2.40	$Ba(Fe_2)[Fe_{1(k)}Cr_{5(k)}Fe_{2(f)}Cr_{1(a)}]\{Fe_1\}O_{19}$
8.0	1.00	—	3.20	3.20	$Ba(Fe_2)[Cr_{6(k)}Fe_{1(f)}Cr_{1(f)}Cr_{1(a)}]\{Fe_1\}O_{19}$
$Li_{0.5}Fe_{2.5-x}Cr_xO_4$					
x	Li_2O_2	Fe_2O_3	Fe	Cr_2O_3	
0	0.25	0.750	1.00	—	$(Fe_1)[Li_{0.5}Fe_{1.5}]O_4$
0.75	0.25	0.375	1.00	0.375	$(Fe_1)[Li_{0.5}Fe_{0.75}Cr_{0.75}]O_4$
1.25	0.25	1.125	1.00	0.625	$(Fe_1)[Li_{0.5}Fe_{0.25}Cr_{1.25}]O_4$
1.50	0.25	—	1.00	0.750	$(Fe_1)[Li_{0.5}Cr_{1.50}]O_4$
1.75	0.25	0.375	1.00[a]	0.375	$(Li_{0.25}Fe_{0.75})[Li_{0.25}Cr_{1.75}]O_4$

[a]Cr instead of Fe for this composition.

Table 2 X-Ray powder diffraction lattice parameter values (±0.004 Å) for $BaFe_{12-x}Cr_xO_{19}$ and $Li_{0.5}Fe_{2.5-x}Cr_xO_4$ produced by SHS. Series 1, zero field SHS followed by annealing at 1200 °C ($BaFe_{12-x}Cr_xO_{19}$) or 1150 °C ($Li_{0.5}Fe_{2.5-x}Cr_xO_4$) for 2 h. Series 2, SHS conducted in a magnetic field of 1.1 T followed by annealing

	Series 1		Series 2	
Formula	*a*/Å	*c*/Å	*a*/Å	*c*/Å
$BaFe_{12}O_{19}$	5.885	23.171	5.889	23.190
$BaFe_{10.0}Cr_{2.0}O_{19}$	5.873	23.093	5.875	23.109
$BaFe_{8.0}Cr_{4.0}O_{19}$	5.860	23.023	5.864	23.067
$BaFe_{6.0}Cr_{6.0}O_{19}$	5.844	22.890	5.851	23.029
$BaFe_{4.0}Cr_{8.0}O_{19}$	5.849	22.830	5.847	22.961
$Li_{0.5}Fe_{2.5}O_4$	8.342	—	8.321	—
$Li_{0.5}Fe_{1.75}Cr_{0.75}O_4$	8.303	—	8.295	—
$Li_{0.5}Fe_{1.25}Cr_{1.25}O_4$	8.297	—	8.281	—
$Li_{0.5}Fe_{1.00}Cr_{1.50}O_4$	8.291	—	8.277	—
$Li_{0.5}Fe_{0.75}Cr_{1.75}O_4$	8.288	—	8.275	—

Fe_2O_3 (2.395 g, 15 mmol) and Cr_2O_3 (1.140 g, 7.5 mmol) were ground together in a pestle and mortar. The resulting powder was placed on a ceramic tile in air and the mixture initiated by means of a nichrome filament at 800 °C. This produced an orange propagation wave (*ca.* 1000 °C) that travelled through the material at *ca.* 2 mm s^{-1}. The powder darkened to black after the propagation wave had passed and became partly fused. The black material both as prepared and after sintering at 1200 °C for 2 h was analysed by X-ray powder diffraction, Table 2, VSM magnetometry, FTIR, SEM/EDXA, electron probe analysis and Mössbauer. The FTIR spectra of the hexagonal ferrites showed a broad band at 600 cm^{-1}. EDXA gave the expected Ba/Cr/Fe ratios for all samples ($BaFe_{12-x}Cr_xO_{19}$).

Preparation of $Li_{0.5}Fe_{2.5-x}Cr_xO_4$ (x = 0, 0.75, 1.25, 1.5, 1.75)

The same general procedure was used in the synthesis for all values of *x* illustrated here for $x = 1.25$ (Table 1).

Li_2O_2 (0.458 g, 10 mmol), iron powder (2.234 g, 40 mmol), Fe_2O_3 (0.799 g, 5 mmol) and Cr_2O_3 (3.800 g, 25 mmol) were ground together in a pestle and mortar. The resulting powder was placed on a ceramic tile in air and the mixture initiated by means of a nichrome filament at 800 °C. This produced an orange–red propagation wave (800 °C) that travelled through the material at *ca.* 1 mm s^{-1}. The powder darkened to black after the propagation wave had passed and became partly fused. The black material both as prepared and after sintering at 1150 °C for 2 h was analysed by X-ray powder diffraction Table 2, VSM magnetometry, FTIR, SEM/EDXA, electron probe analysis and Mössbauer spectroscopy. The FTIR spectra showed overlapping broad bands centered at 630 and 480 cm^{-1}. EDXA gave the expected Cr/Fe ratios for all samples.

Note for the composition $x = 1.75$, chromium powder was used instead of iron.

Reactions in a magnetic field

The same reactions to form $BaFe_{12-x}Cr_xO_{19}$ ($x = 0$, 2, 4, 6, 8) and $Li_{0.5}Fe_{2.5-x}Cr_xO_4$ ($x = 0$, 0.75, 1.25, 1.5, 1.75) were also studied in a magnetic field of 1.1 T by placing the reacting powders in a 22 mm od quartz tube. Reactions were initiated by means of a heated filament. Some structuring of the product was noted in the magnetic field, with two horizontal grooves in the top and bottom of the powder which corresponded to some preorganisation of the powder prior to SHS. The SHS reactions in a magnetic field had faster propagation velocity (5 mm s^{-1}) and higher synthesis wave temperatures (*ca.* 1200 °C for $BaFe_{12-x}Cr_xO_{19}$ and *ca.* 925 °C for $Li_{0.5}Fe_{2.5-x}Cr_xO_4$) than those conducted in zero field. The powders produced from the SHS reactions in a magnetic field were ground and sintered at 1200 °C ($BaFe_{12-x}Cr_xO_{19}$) or 1150 °C ($Li_{0.5}Fe_{2.5-x}Cr_xO_4$) for 2 h. The samples were analysed by X-ray powder diffraction Table 2, VSM magnetometry, FTIR, SEM/EDXA, and Mössbauer. The FTIR spectra of the hexagonal ferrites showed a broad band at 600 cm^{-1}. EDXA gave the expected Ba/Cr/Fe ($BaFe_{12-x}Cr_xO_{19}$) and Cr/Fe ($Li_{0.5}Fe_{2.5-x}Cr_xO_4$) ratios.

All samples prepared in a magnetic field are known as series 2 materials in subsequent analysis and discussions.

Caution: SHS reactions can be very exothermic, sometimes explosively, with any new system care should be taken to carry the reactions out behind a blast proof screen. High temperature material can be ejected from the site of a laboratory scale reaction up to 1 m.

Results

Sample preparation

SHS reactions were performed by using various starting mixtures of Fe_2O_3, BaO_2 (or Li_2O_2), Fe and Cr_2O_3. The molar ratio of each reagent was chosen to conform with the stoichiometry in the products (Table 1). In all reactions a slight excess of the barium peroxide was used. At stoichiometric levels of barium the hexagonal ferrites ($BaFe_{12-x}Cr_xO_{19}$) also contained some iron oxide. The use of excess barium in the reaction mirrors our initial findings for the synthesis of $SrFe_{12}O_{19}$[24] and conventional ceramics methods where typically a 1:11 molar ratio of barium to iron is used.[27] The reaction was driven by the exothermic oxidation of Fe metal, co-added metal oxides act as heat sinks to stop the reaction becoming too exothermic; whilst also being incorporated in the product. Barium peroxide and Li_2O_2 act as internal intimately mixed sources of oxygen and also provide barium and lithium. The peroxides were used in preference to the carbonates of these elements which are used in traditional synthesis of ferrites as the peroxides provide a superior source of oxygen and also avoid potential carbon contamination. In the case of $BaFe_{10}Cr_2O_{19}$ and $Li_{0.5}Fe_{1.5}Cr_{1.0}O_4$ the reagent mixes were:

$$BaO_2 + 2.5Fe_2O_3 + Cr_2O_3 + 5Fe + 3.25O_2 \rightarrow BaFe_{10}Cr_2O_{19}$$

$$Li_2O_2 + Fe_2O_3 + 4Fe + 2Cr_2O_3 + 2.5O_2 \rightarrow 4Li_{0.5}Fe_{1.5}CrO_4$$

Two different series of samples were prepared for both $BaFe_{12-x}Cr_xO_{19}$ and $Li_{0.5}Fe_{2.5-x}Cr_xO_4$: series 1, the zero field SHS product subsequently sintered at 1200 °C ($BaFe_{12-x}Cr_xO_{19}$) or 1150 °C ($Li_{0.5}Fe_{2.5-x}Cr_xO_4$) for 2 h; series 2, the product of an SHS reaction carried out in an applied field of 1.1 T followed by sintering at 1200 °C ($BaFe_{12-x}Cr_xO_{19}$) or 1150 °C ($Li_{0.5}Fe_{2.5-x}Cr_xO_4$) for 2 h. It should be noted that the reactions were all carried out in air. The limiting reagent in the reactions studied here was the diffusion of oxygen into the reacting powders. This meant that in most cases the reaction proceeded by an orange–red propagation wave (*ca.* 900 °C) of width 1–2 mm and velocity *ca.* 1–2.0 mm s^{-1}. In all reactions the product was a black–brown material. It was observed that the propagation wave temperature and velocity were increased for the reactions that were carried out in the presence of a magnetic field.

The SHS preparation of chromium substituted lithium and barium ferrites is straightforward and rapid. The reaction is over in about 30 s. Traditional methods to these materials involve the use of ball-mills to grind the reagents[25] or precipitation synthesis in which up to eight individual reactions steps involving gel-growth and concentrated acids are used.[26] The products from such reactions are then heat treated at 1150–1200 °C for prolonged time periods. The SHS products for both hard and soft ferrites are equal in quality to any conventionally prepared material and somewhat easier to

obtain. Further the synthesis reported here is very unusual for the preparation of complex oxide materials by SHS; usually a pressurised oxygen atmosphere is required using special reaction vessels. The reactions studied here in air are extremely easy to perform and use inexpensive apparatus (the reactions can be initiated by a match on a ceramic bathroom tile).

Characterisation

X-Ray powder data were recorded for all the unsintered and sintered SHS products and analysed using Philips proprietary software. The unsintered products showed predominantly $BaFe_{12-x}Cr_xO_{19}$ and $Li_{0.5}Fe_{2.5-x}Cr_xO_4$ respectively, with small amounts of metal oxide impurities such as $LiFeO_2$, Fe_2O_3 and Cr_2O_3, overall amounting to *ca.* 10 wt.% of the material. The presence of these materials shows incomplete reaction during the SHS stage, although as sintering largely removed these impurities we infer that $BaFe_{12-x}Cr_xO_{19}$ and $Li_{0.5}Fe_{2.5-x}Cr_xO_4$ are the favored thermodynamic products. X-Ray data for the sintered products showed hexagonal structures for $BaFe_{12-x}Cr_xO_{19}$ and cubic spinel structures for $Li_{0.5}Fe_{2.5-x}Cr_xO_4$ as shown in Fig. 1(a) and (b), with lattice parameters as given in Table 2. In some of the Cr-rich zero field SHS samples of both the Ba and Li ferrites a trace amount of iron oxide impurity was noted even after sintering. A general decrease in lattice parameters with increasing Cr substitution was noted for both $BaFe_{12-x}Cr_xO_{19}$ and $Li_{0.5}Fe_{2.5-x}Cr_xO_4$ series, which mirrors previous studies of conventionally prepared materials.[28,29] This variation in unit cell size may be attributed to the slightly smaller ionic radii of six-fold coordinated Cr^{3+} compared to that of six-fold high spin Fe^{3+}.[30] In the $Li_{0.5}Fe_{2.5-x}Cr_xO_4$ series ($x>0.5$) no evidence for superlattice structures was evident. This indicates, for example, that in the compound $Li_{0.5}Fe_{2.0}Cr_{0.5}O_4$ the lithium, chromium and iron atoms are randomly arranged on the octahedral sublattice rather than in an ordered arrangement.

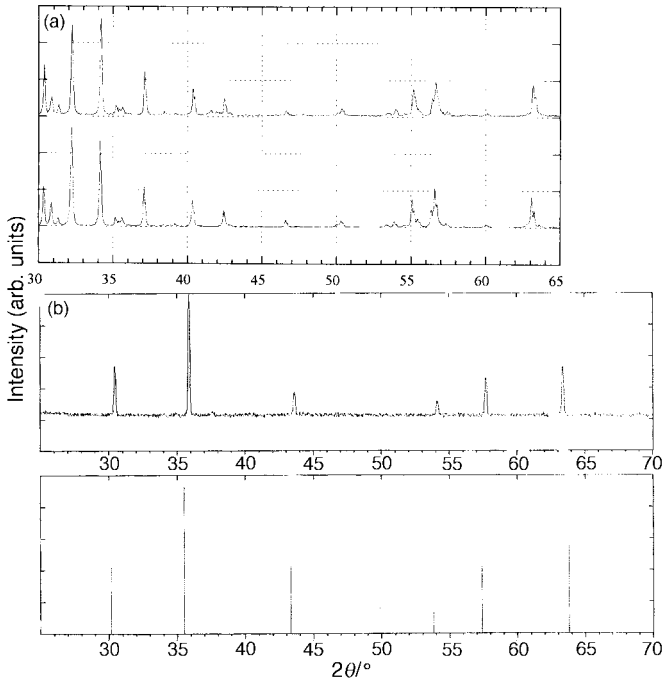

Fig. 1 (a) Upper trace: X-ray powder diffraction pattern obtained from the SHS reaction of BaO_2, Fe_2O_3, Fe and Cr_2O_3 (1.00 : 1.60 : 4.80 : 0.80 molar ratio) after sintering at 1200 °C for 2 h. Lower trace: X-ray powder diffraction pattern of a commercial sample of $BaFe_{12}O_{19}$. (b) Upper trace: X-ray powder diffraction pattern obtained from the SHS reaction of Li_2O_2, Fe_2O_3, Fe and Cr_2O_3 (0.25 : 0.375 : 1.00 : 0.375 molar ratio) after sintering at 1150 °C for 2 h ($Li_{0.5}Fe_{1.75}Cr_{0.75}O_4$). Lower trace: literature stick pattern for $Li_{0.5}Fe_{2.5}O_4$.[26]

The lower limit on the crystallite sizes for both the as prepared and sintered $BaFe_{12-x}Cr_xO_{19}$ and $Li_{0.5}Fe_{2.5-x}Cr_xO_4$ materials was found to be of order 110 nm, as determined by the Scherrer equation[31] from the line broadening, neglecting strain effects.

SEM micrographs of the sintered $BaFe_{12-x}Cr_xO_{19}$ samples showed hexagonal crystallites of size *ca.* 1.0 μm and the $Li_{0.5}Fe_{2.5-x}Cr_xO_4$ samples showed cubic crystallites of size *ca.* 1.1 μm. As the dimensions are larger than that obtained from the X-ray data, this implies that there may be twinning and other structural defects present in the grains. Electron microprobe results for sintered $Li_{0.5}Fe_{2.5-x}Cr_xO_4$ ($x=0.25$, 1.00 and 1.50) (series 1) samples showed a homogeneous material with the expected Fe : Cr ratios. EDAX was also consistent for $BaFe_{12-x}Cr_xO_{19}$ and $Li_{0.5}Fe_{2.5-x}Cr_xO_4$ for both the series 1 and 2 materials with the expected Ba : Fe : Cr and Fe : Cr ratios. No evidence of phase segregation or uneven chromium substitution was observed for either sets of sintered materials by EDAX.

The FTIR spectra of both $BaFe_{12-x}Cr_xO_{19}$ and $Li_{0.5}Fe_{2.5-x}Cr_xO_4$ series 1 and 2 samples match those of conventionally prepared materials and literature standards.[32] The FTIR spectra of $BaFe_{12-x}Cr_xO_{19}$ showed a broad band centered at 600 cm^{-1} attributable to overlapping Fe–O and Cr–O stretches. Some changes in the shoulders of the broad bands were noted with Cr substitution. The FTIR spectra of spinel ferrites such as $Li_{0.5}Fe_{2.5-x}Cr_xO_4$ have been extensively investigated.[33] Most of these materials show strong overlapping absorptions in the region 800–400 cm^{-1}. These have been attributed to Fe–O and Cr–O stretches as well as Li–O vibrations. The precise nature of the absorptions has also been related to the degree of crystallographic ordering of the lithium, chromium and iron atoms within the structure.[32] As has been noted above, chromium substitution into SHS prepared $Li_{0.5}Fe_{2.5}O_4$ goes onto the octahedral sublattice. IR data for these compounds match most closely those materials in which there is a random distribution of the Cr, Fe and Li atoms within the octahedral sublattice.[32] This is somewhat different to most traditionally prepared spinels where the longer synthesis times allow for local ordering of the atoms on the octahedral sites. Indeed the IR data tie in with the X-ray data where no superlattice lines were observed for the $Li_{0.5}Fe_{2.5-x}Cr_xO_4$ ($x>0.5$) series.

^{57}Fe Mössbauer absorption spectra were recorded for $BaFe_{12-x}Cr_xO_{19}$ [Fig. 2(a) and (b)] and $Li_{0.5}Fe_{2.5-x}Cr_xO_4$ [Fig. 3(a) and (b)] series 1 and 2 at room temperature. The spectra were least squares fitted using Lorentzian lineshapes and assumed a first order perturbation approach to the combination of electric quadrupole and magnetic interactions. For $BaFe_{12-x}Cr_xO_{19}$ the spectra were analysed as the sum of four subcomponent spectra, attributed to the five crystallographically distinct Fe sites in the Ba ferrite lattice: 2a, $4f_{iv}$, $4f_{vi}$, 2b, and 12k. As the 2a and $4f_{iv}$ sites have similar Mössbauer parameters, these were convoluted into one subcomponent. The distinction between these subspectra is illustrated for the case of $BaFe_{12}O_{19}$ in Fig. 4(a). In a similar manner the $Li_{0.5}Fe_{2.5-x}Cr_xO_4$ spectra were fitted with two subcomponent spectra attributed to the octahedral and tetrahedral Fe sites, as illustrated in Fig. 4(b) for pure $Li_{0.5}Fe_{2.5}O_4$. Additionally a third component due to paramagnetic iron was fitted in the $Li_{0.5}Fe_{2.5-x}Cr_xO_4$ series. The origin of this component is discussed in more detail below.

Hysteresis loops were recorded on all the samples in fields up to 7.5 kOe at room temperature. Representative hysteresis loops are shown in Fig. 5(a) and (b). The variation in maximum magnetisation σ_{max}, remanent magnetisation σ_r and coercive force H_c with chromium substitution for $BaFe_{12-x}Cr_xO_{19}$ and $Li_{0.5}Fe_{2.5-x}Cr_xO_4$ samples prepared in zero and applied magnetic fields are shown in Fig. 6. Samples prepared in a magnetic field (series 2) showed significant

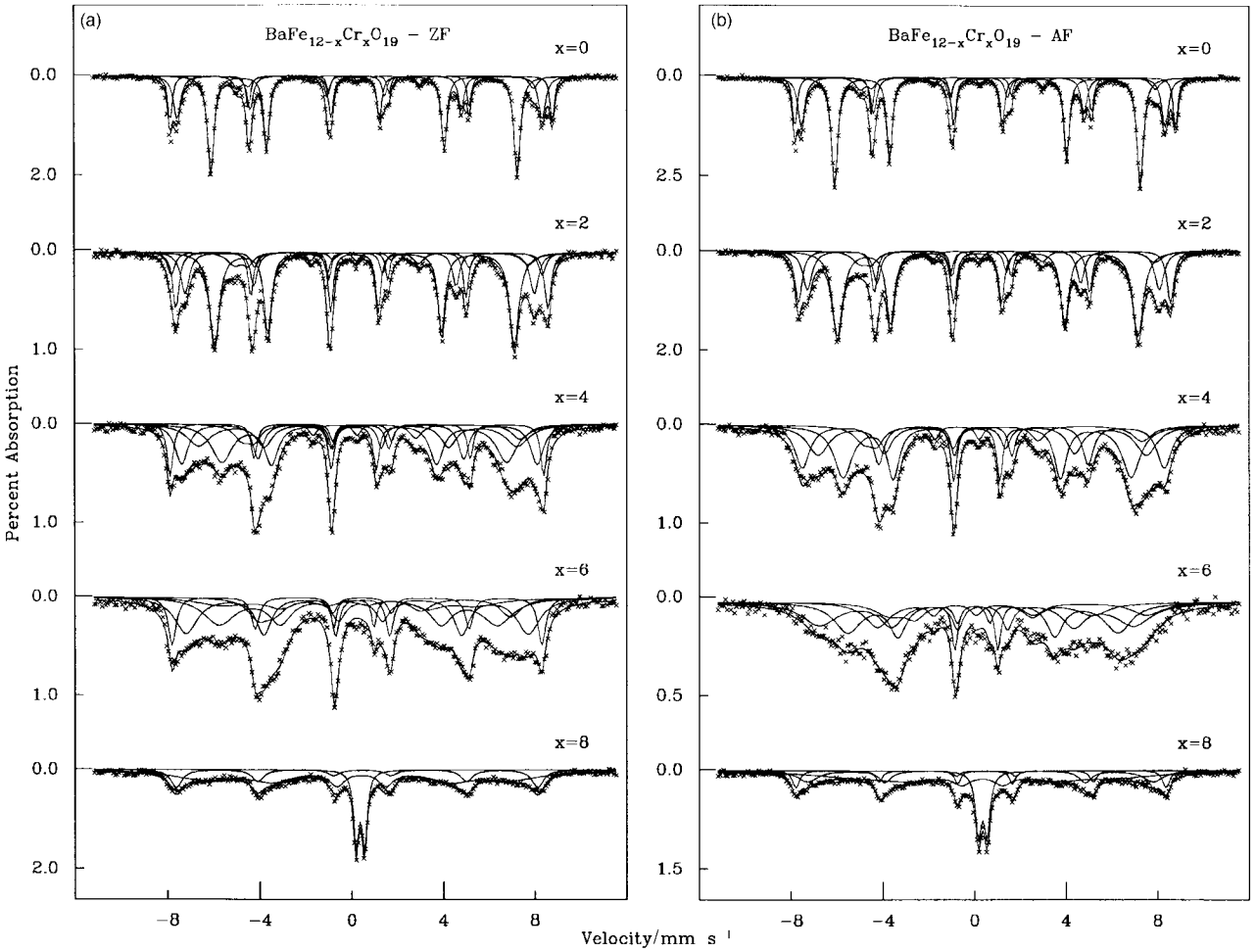

Fig. 2 (a) Room temperature Mössbauer spectra of $BaFe_{12-x}Cr_xO_{19}$ prepared by SHS in air after sintering at 1200 °C for 2 h. (b) Room temperature Mössbauer spectra of $BaFe_{12-x}Cr_xO_{19}$ prepared by SHS in air in a field of 1.1 T after sintering at 1200 °C for 2 h.

differences in σ_{max}, σ_r and H_c compared to samples that were prepared in the absence of a field. It should be noted that these changes occur in materials that had been repowdered and sintered, thus indicating that the magnetic field effects on the SHS prepared powders carry through even after post production steps.

Discussion

Mössbauer measurements: $BaFe_{12-x}Cr_xO_{19}$

^{57}Fe Mössbauer absorption spectra for the SHS prepared barium chromium ferrites are shown in Fig. 2(a) and (b), along with solid lines corresponding to the least squares fits to the data. Similar trends are apparent in both the zero field and applied field SHS samples as a function of Cr substitution, with the magnetic hyperfine sextets of the component subspectra collapsing towards a central quadrupole split doublet as the Cr content increased. Only minor differences are discernible between the two series of samples, the most obvious being the presence of an additional sextet in the zero field $x=6$ sample, evidenced by the sharp absorption peaks in the outermost wings of the spectrum. This component has Mössbauer parameters consistent with hematite, α-Fe_2O_3, and is indicative of a minority fraction of unreacted iron oxide in this sample. Small amounts of hematite impurity were also noted in the zero field $x=2$ and $x=4$ samples.

In fitting the Mössbauer spectra the relative areas of component subspectra were 12:4:4:2:2 for the 12k, $4f_{iv}$, $4f_{vi}$, 2a and 2b sites in pure $BaFe_{12}O_{19}$. Subsequent substitution of iron by chromium in the system can be related primarily to displacement of Fe from the octahedral 12k, $4f_{iv}$ and 2a sites, since Cr^{3+} prefers octahedral sites due to crystal field effects. However, the details of this substitutional process as a function of Cr content are the subject of some controversy.[28,34] Most authors agree about the substitution of Fe in octahedral sites by Cr, but some state that the 2a is substituted initially, and others the 12k sites, and others that the cations are distributed randomly within both the 12k and 2a sites. In fitting the spectra in Fig. 2(a) all three of these models were tested, and the relative goodness of fit parameters compared between the results. We found that there was a slight preference for the model in which the Fe octahedral sites are substituted preferentially, with Cr first occupying the 2a sites, then the 12k sites, and then finally the $4f_{iv}$ sites. These site occupancies are summarised in Table 1.

The hyperfine fields as fitted for the zero field and applied field SHS samples are shown graphically in Fig. 7. The data for the $x=8$ sample are not shown as in that case the collapse of the hyperfine fields towards a paramagnetic doublet makes the different subspectra difficult to distinguish. The same is true to a lesser extent for the $x=6$ spectra. On inspection of Fig. 7 it is clear that all the sites exhibit a systematic decrease in hyperfine field with the addition of chromium, consistent with disruption of the exchange interactions in the lattice. Minor differences are apparent between the zero field and applied field $x=2$ and $x=4$ samples, with the applied field samples having larger hyperfine fields that their zero field counterparts.

Magnetic measurements: $BaFe_{12-x}Cr_xO_{19}$

Of the five different crystallographic sites for the iron atoms in $BaFe_{12}O_{19}$,[24] the octahedral 12k and 2a sites and the five

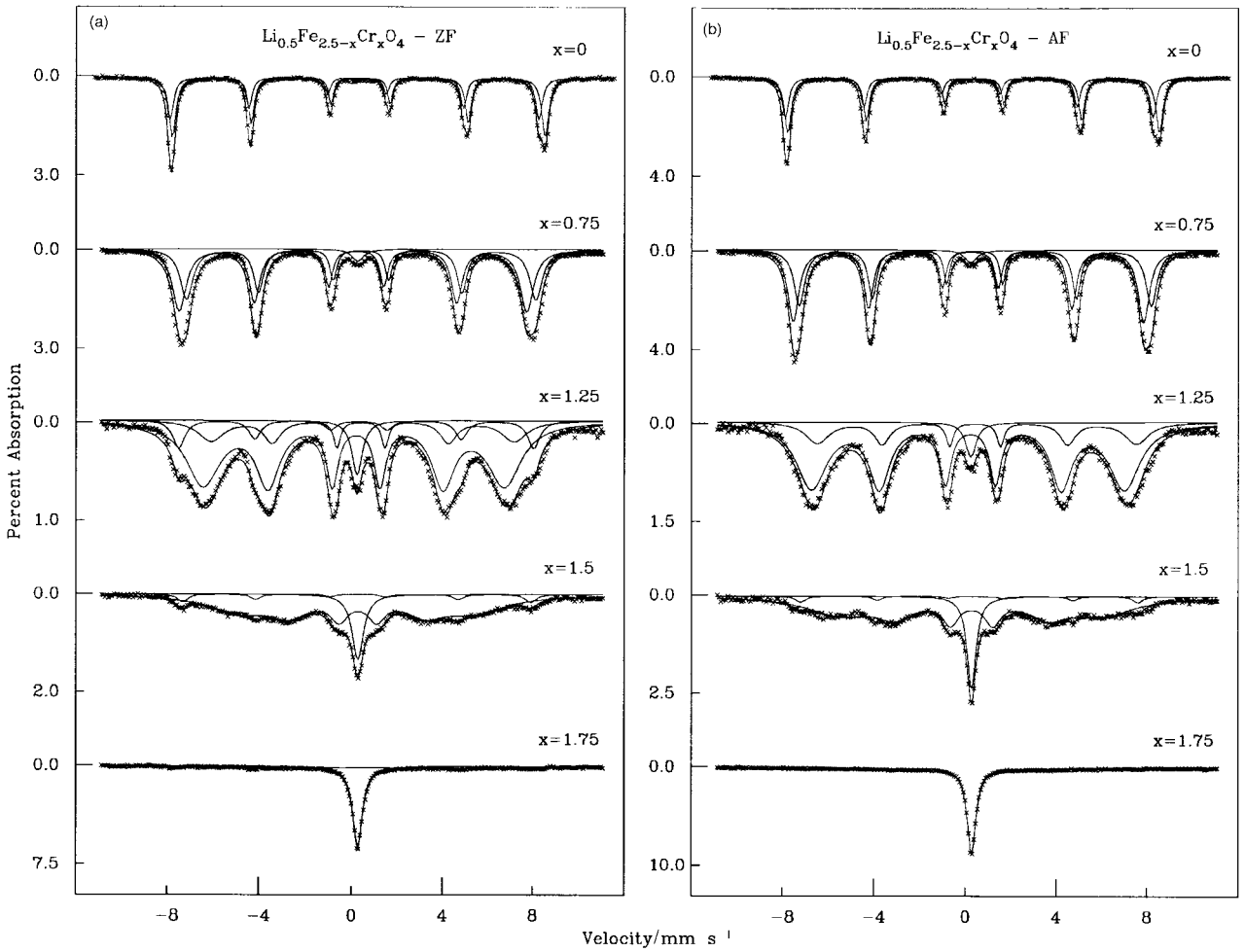

Fig. 3 (a) Room temperature Mössbauer spectra of $Li_{0.5}Fe_{2.5-x}Cr_xO_4$ prepared by SHS in air after sintering at 1150 °C for 2 h. (b) Room temperature Mössbauer spectra of $Li_{0.5}Fe_{2.5-x}Cr_xO_4$ prepared by SHS in air in a field of 1.1 T after sintering at 1150 °C for 2 h.

fold 2b sites are spin up, while the octahedral $4f_{iv}$ and tetrahedral $4f_{vi}$ sites are spin down. Thus, on the basis of the Cr site substitution model outlined above one would expect a steady decrease in saturation magnetisation as a function of Cr up to $x=7$, filling the 2a and 12k sites, then a levelling off above $x=7$ as the $4f_{iv}$ sites are occupied. Such behaviour is indeed seen in the zero field and applied field samples (Fig. 6) for both the maximum magnetisation and the remanent magnetisation, although the approach to paramagnetic behaviour with increasing Cr content is a contributing factor to the shape of the curves. It is notable that at all compositions the magnetisations in the applied field SHS samples are greater than in the corresponding zero field SHS samples.

The coercive forces measured for the samples are also shown in Fig. 6. The applied field SHS samples all have coercivities of order 40–50% less than their zero field SHS counterparts. The origin of this effect is currently under investigation in our laboratory. Given the similar Mössbauer, X-ray, SEM and EDAX data for equivalent compositions between the two series of materials, it is most likely to be due to changes in microstructure and/or changes in magnetic domain size, rather than compositional or substitutional variations.

Mössbauer measurements: $Li_{0.5}Fe_{2.5-x}Cr_xO_4$

Mössbauer spectra of the SHS prepared lithium chromium ferrites are shown in Fig. 3(b), along with their least squares fits. In both series of samples the effect of increasing Cr substitution is the collapse of the magnetic sextet subspectra into a central paramagnetic singlet. This singlet is also seen to coexist with the magnetic sextets in all the Cr-substituted samples. Minor differences between the zero field and applied field samples are evident for $x=1.25$ and $x=1.5$; in both cases the zero field spectra show an additional sextet with outermost peaks in the wings of the spectrum. The Mössbauer parameters of this sextet are not immediately recognisable as due to an impurity: the hyperfine field, of order 48 T, is too small to be due to an iron oxide. Also the X-ray diffraction patterns for both these sample show no sign of any impurities. It therefore appears to be an intrinsic effect in the substituted material, although the exact origin of the component is not yet fully identified.

In fitting the Mössbauer spectra a simple model was adopted using two overlapping sextets for the tetrahedral and octahedral coordination sites for iron, constrained with relative areas proportional to the occupancies as stated in Table 1. On the basis of crystal field effects the Cr^{3+} ions are assumed to preferentially displace initially Fe^{3+} and then Li^+ from octahedral sites in the spinel. It may be noted that in the literature some authors have used more detailed models, including multiple sets of component subspectra, to model lithium ferrite and its substituted variants taking into account the perturbing effect of the 1:3 mixture of Li^+ and Fe^{3+} ions on the octahedral sublattice.[35,36] We choose not to use such involved models at present. The Mössbauer parameters obtained for the spectra agree well with previous measurements on conventionally prepared materials, with isomer shifts δ at *ca.* 0.38 and 0.20 mm s^{-1} for the octahedral and tetrahedral sites respectively, quadrupole shifts near zero for both, and hyperfine fields in the pure lithium ferrite of 50.5 and 50.0 T respectively. The latter result, coupled with the absence of any

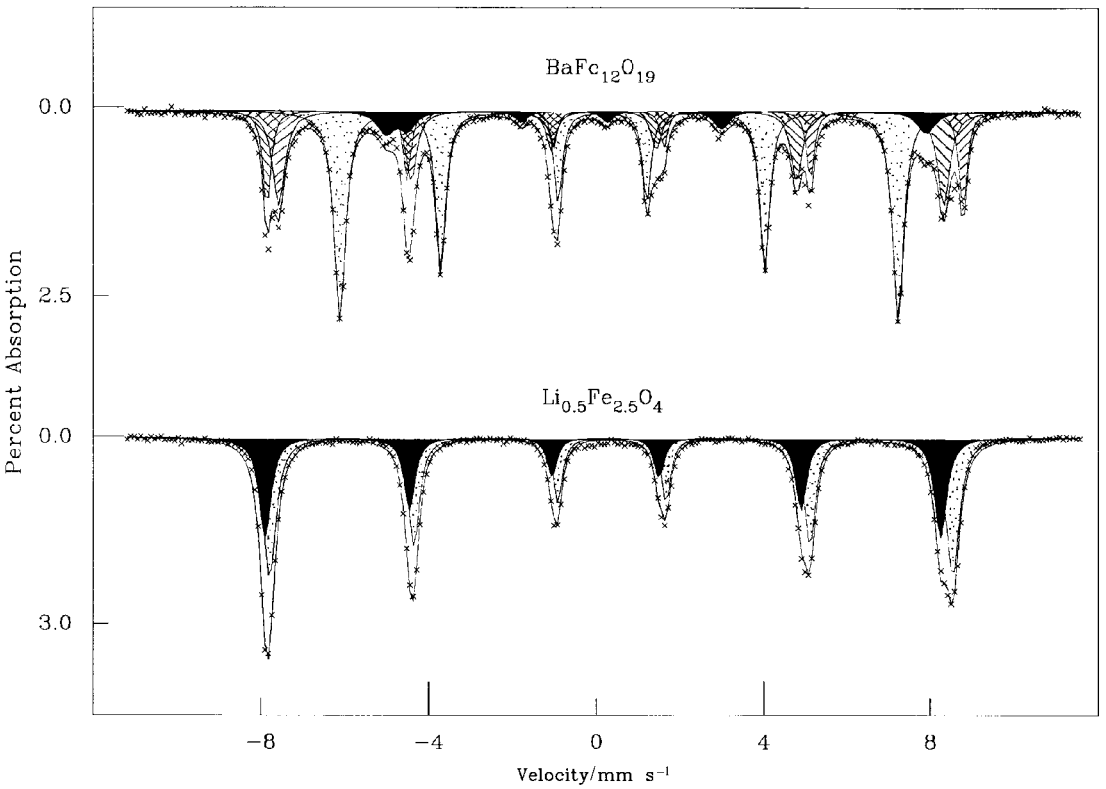

Fig. 4 Upper trace: Mössbauer spectra of $BaFe_{12}O_{19}$ showing the five subspectra corresponding to the (▨) 12k, (▨) $4f_{iv}$, (▨) $4f_{vi}$, (▨) 2a and (■) 2b sublattice sites; lower trace: Mössbauer spectra of $Li_{0.5}Fe_{2.5}O_4$ showing the two subspectra corresponding to (▨) octahedral and (■) tetrahedral sublattice sites.

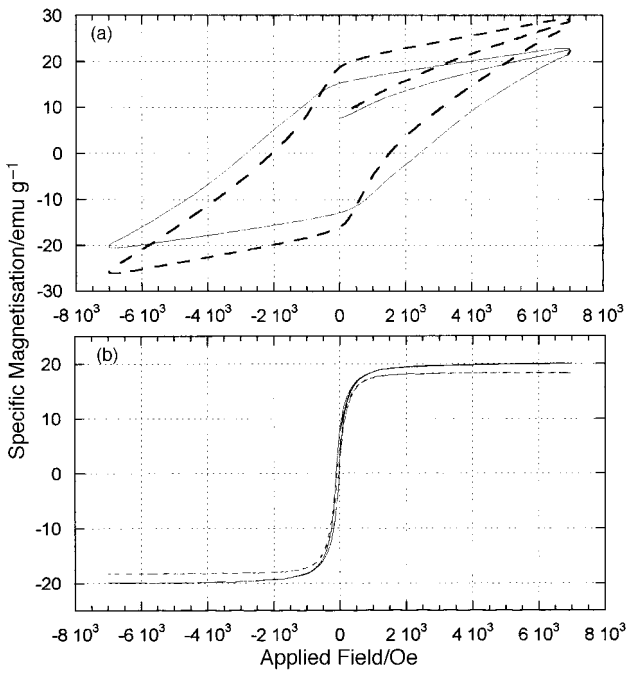

Fig. 5 Room temperature hysteresis loops for sintered $BaFe_{10}Cr_{19}$ prepared in the absence of a magnetic field (—) and in the presence of a magnetic field (– – –). (b) Room temperature hysteresis loops for sintered $Li_{0.5}Fe_{1.75}Cr_{0.75}O_4$ materials prepared in the absence of a magnetic field (—) and in the presence of a magnetic field (– – –).

superstructure lines visible in the X-ray data, indicates that at least in the pure ferrite the lithium atoms are randomly distributed over the octahedral sites.[37]

As the amount of Cr substitution increases, the Fe occupancy of the octahedral sites falls. This is evident in Fig. 3(a) and (b) with the decreasing relative intensity of the component sextet with the larger isomer shift. A paramagnetic singlet component is also observed as chromium is introduced. The intensity of this singlet increases with Cr^{3+} concentration, coexisting with the magnetic sextets for $x=0.75$, 1.25 and 1.5. Such features have been observed in other substituted ferrites,[38] and may be attributed to inhomogeneous Cr substitution leading to some of the Fe atoms becoming isolated from the majority of exchange coupled Fe atoms. This in turn results in paramagnetic behaviour, in the case of individual atoms, or superparamagnetic behaviour, in the case of clusters, either of which can give rise to a singlet in the spectra. The largest changes in the Mössbauer spectra occur at $x=1.5$ and 1.75 and correspond to the complete replacement of iron by chromium in the octahedral sites.

Magnetic measurements: $Li_{0.5}Fe_{2.5-x}Cr_xO_4$

The introduction of Cr^{3+} ions into lithium ferrite strongly affects the magnetic parameters of the system. Trends are observed with σ_{max} and σ_r decreasing and H_c increasing with chromium substitution, as shown in Fig. 6. The decrease in magnetisation corresponds to the collapse in Mössbauer hyperfine fields, and is largely due to the increasing fluctuations in the Fe moments as the increasing Cr concentration disrupts the interatomic exchange interactions. Some small differences in the magnetic parameters are seen for the zero field and applied field SHS samples, with the coercive force showing the largest and most systematic changes. This is reminiscent of the effects seen in the barium chromium ferrites (although in the opposite direction), and implies that similar processes may be involved.

Effects of an external magnetic field on SHS reactions

In general use of a magnetic field during SHS can have a number of effects. It can orient the reacting particles and products along magnetic field lines. It can also affect the

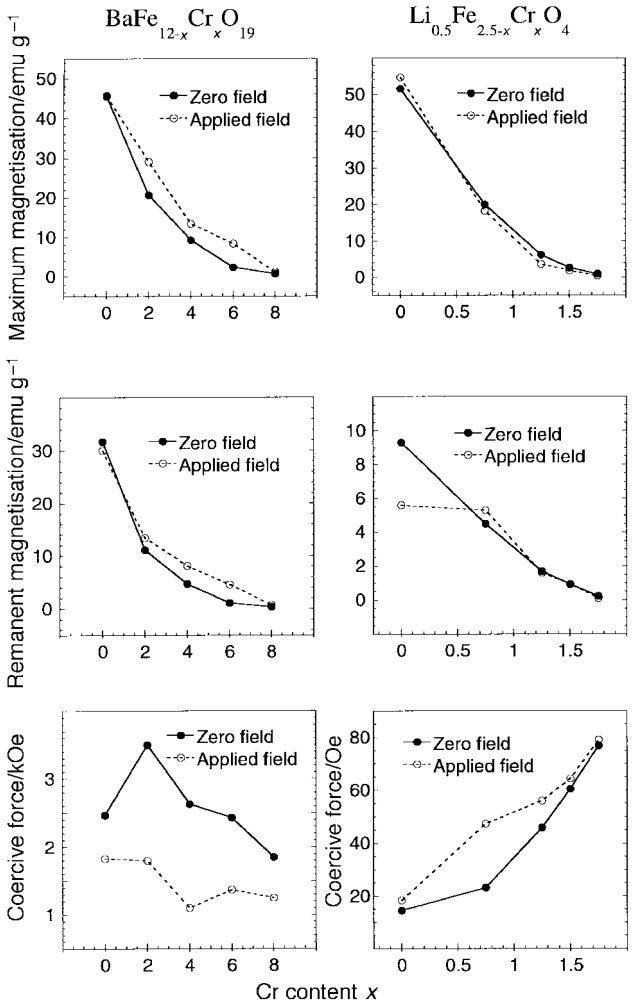

Fig. 6 Magnetic properties of $BaFe_{12-x}Cr_xO_{19}$ and $Li_{0.5}Fe_{2.5-x}Cr_xO_4$ prepared by SHS; maximum magnetisation σ_{max} (± 0.1 emu g^{-1}); remanent magnetisation σ_r (± 0.1 emu g^{-1}), and coercive force H_c (± 10 Oe) measured at 7.5 kOe at room temperature. Series 1 (closed circles) zero field SHS followed by annealing at 1200 °C ($BaFe_{12-x}Cr_xO_{19}$) or 1150 °C ($Li_{0.5}Fe_{2.5-x}Cr_xO_4$) for 2 h and series 2 (open circles) SHS conducted in a magnetic field of 1.1 T followed by annealing.

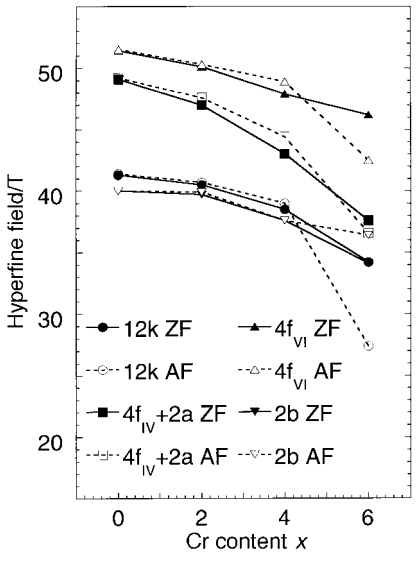

Fig. 7 Plot of hyperfine fields (T) against chromium content for the different sublattice sites in $BaFe_{12-x}Cr_xO_{19}$ ($x=0$, 2, 4, 6), as determined from the room temperature Mössbauer spectra.

velocity and temperature of the combustion wave since magnetic components are oriented rather than being randomly distributed. The alignment of the grains may increase the interfacial contact between the reacting species and account for the faster reaction rate. Since the SHS reaction proceeds by a molten reaction zone moving through the solid it is also possible that the magnetic field could draw magnetic components such as iron metal into the reaction zone, increasing the propagation rate. In the case of barium chromium ferrites we observed that the SHS reactions in a magnetic field had significantly faster propagation velocity and higher synthesis wave temperatures than the zero field reactions. It is notable that the applied field samples showed no signs of unreacted hematite impurities, as some of the zero field samples did, supporting the hypothesis of a more complete reaction being facilitated by the applied field. It is certain that the magnetic domain structure of the post-SHS product is more orientated in the applied field case. It is likely that a memory of this is retained even after the samples are broken up and powdered, and that this carries over into the sintered materials in the form of reduced coercive forces.

Conclusions

Representative hard ($BaFe_{12-x}Cr_xO_{19}$) and soft ($LiFe_{2.5-x}Cr_xO_4$) ferrites were synthesized for the first time by self-propagating high-temperature synthesis (SHS) in air. The reactions are straightforward, easy to perform and offer significant reductions in synthesis time and external energy input compared to conventional synthesis. Despite the short time period of the SHS reaction and subsequent sintering, homogeneous single phase products were produced which had magnetic characteristics equal to those prepared by traditional methods. Reactions carried out in a magnetic field had significantly faster propagation velocity and higher temperatures than those in zero field. This resulted in major perturbations in Mössbauer and magnetic measurements for samples prepared in a magnetic field. These adjustments in absolute values cannot be explained by changes in site occupancy and are most likely related to changes in magnetic microstructure.

Dr. M. Kuznetsov thanks the Royal Society for an FSU fellowship. Dr. I. P. Parkin and Dr. Q. A. Pankhurst thank the Royal Society for an FSU Joint Project Grant. Dr. Y. Morozov is thanked for useful discussions. Mössbauer spectra were collected under the auspicies of the University of London Intercollegiate Research Service.

References

1 C. N. R. Rao and J. Gopalakrishnan, *New Directions in Solid State Chemistry*, Cambridge University Press, Cambridge, 1997, p. 122.
2 H. Yanagida, K. Koumoto and M. Migayuma, *The Chemistry of Ceramics*, J. Wiley and Sons, Chichester, 1996, p. 97.
3 K. J. Rao, *Perspectives in Solid State Chemistry*, Narosa Publishing House, New Delhi, 1995, p. 39.
4 D. Segal, *Chemical Synthesis of Advanced Ceramic Materials*; *Chemistry of Solid State Materials*, ed. A. R. West and H. Baxter, Cambridge University Press, Cambridge, 1989, p. 33; J. Livage, *Curr. Opin. Solid State Mater. Sci.*, 1997, **2**, 132.
5 M. Ricard-Poulet and S. Vilminot, *J. Mater. Chem.*, 1998, **8**, 131.
6 I. P. Parkin and A. T. Rowley, *J. Mater. Chem.*, 1995, **5**, 909; I. P. Parkin, *Chem. Ind. (London)*, 1997, 725.
7 A. G. Merzhanov, *Adv. Mater.*, 1992, **4**, 294; *Int. J. Self-Propag. High Temp Synth.*, 1995, **4**, 323.
8 I. P. Parkin, *Chem. Soc. Rev.*, 1996, 199.
9 P. R. Bonneau, R. F. Jarvis and R. B. Kaner, *Nature*, 1991, **349**, 510.
10 A. G. Merzhanov and I. P. Borovinskaya, *Combust. Sci. Technol.*, 1975, **10**, 827.
11 B. Z. Shakhashiri, *Chemical Demonstrations, a Handbook for*

Teachers of Chemistry, University of Wisconsin Press, London, 1983, vol. 1, p. 85.
12 A. G. Merzhanov, *J. Mater. Process. Technol.*, 1996, **56**, 222.
13 M. D. Nersesyan, *Neorg. Khim.*, 1984, **29**, 860.
14 V. N. Bloshenko, V. A. Bokii, I. P. Borovinskaya and V. I. Boyarchenko, *Dokl. Akad. Nauk. USSR*, 1992, **324**, 1046.
15 A. S. Mukasyan and I. P. Borovinskaya, *Int. J. Self-propag. High-Temp. Synth.*, 1992, **1**, 55.
16 A. G. Merzhanov, *Int. J. Self-propag. High-Temp. Synth.*, 1997, **6**, 119; R. Orru, B. Simoncini, P. F. Virdis and G. Cao, *Int. J. Self-Propag. High-Temp. Synth.*, 1995, **4**, 137.
17 R. Pampuch, *Int. J. Self-propag. High-Temp. Synth.*, 1997, **6**, 187.
18 J. B. Wiley and R. B. Kaner, *Science*, 1992, **255**, 1093; R. E. Treece, G. S. Macala, L. Rao, D. Franke, H. Eckert and R. B. Kaner, *Inorg. Chem.*, 1993, **32**, 2745; R. E. Treece, G. S. Macla and R. B. Kaner, *Chem. Mater.*, 1992, **4**, 9; E. G. Gillan and R. B. Kaner, *Inorg. Chem.*, 1994, **33**, 5693; L. Rao and R. B. Kaner, *Inorg. Chem.*, 1994, **33**, 3210.
19 A. L. Hector and I. P. Parkin, *J. Chem. Soc.*, *Chem. Commun.*, 1993, 1096; J. C. Fitzmaurice, A. L. Hector and I. P. Parkin, *J. Chem. Soc., Dalton Trans.*, 1993, 243; A. L. Hector and I. P. Parkin, *J. Mater. Chem.*, 1994, **4**, 279; J. C. Fitzmaurice and I. P. Parkin, *New J. Chem.*, 1994, **18**, 825; S. Ali, M. D. Aguas, A. L. Hector, G. Henshaw and I. P. Parkin, *Polyhedron*, 1997, **16**, 3635.
20 A. L. Hector and I. P. Parkin, *J. Chem. Mater.*, 1995, **7**, 1728.
21 Z. A. Munir, *Int. J. Self-Propag. High-Temp. Synth.*, 1997, **6**, 165.
22 K. C. Patil, S. T. Aruna and S. Ekambaram, *Curr. Opin. Solid State Mater. Sci.*, 1997, **2**, 158.
23 A. G. Merzhanov, *Adv. Powder Metall. Particulate Mater.*, 1992, **9**, 341.
24 H. Hibst, *Angew. Chem.*, *Int. Ed. Engl.*, 1982, **21**, 270.
25 G. Elwin, I. P. Parkin, Q. T. Bui, L. Fernandez Barquin, Q. A. Pankhurst, A. V. Komarov and Y. G. Morozov, *J. Mater. Sci. Lett.*, 1997, **16**, 1237; G. Elwin, I. P. Parkin, Q. T. Bui, L. Fernandez Barquin, Q. A. Pankhurst, A. V. Komarov and Y. G. Morozov, *Adv. Mater.*, 1997, **9**, 643; G. Elwin, I. P. Parkin, Q. T. Bui, L. Fernandez Barquin, Q. A. Pankhurst, A. V. Komarov and Y. G. Morozov, *J. Mater. Chem.*, 1998, **8**, 573.
26 K. Heneda and H. Kojima, *Jpn. J. Appl. Phys.*, 1973, **12**, 355; H. Yang, Z. Wang, M. Zhao, J. Wang, D. Han, H. Luo and L. Wang, *Mater. Chem. Phys.*, 1997, **48**, 60.
27 S. C. Teng, Y. T. Chien and T. C. Ko, *J. Mater. Sci. Lett.*, 1995, **14**, 519.
28 E. F. Bertaut, A. Deschamps and R. Pauthenet, *J. Phys. Radium*, 1959, **20**, 404.
29 E. W. Gorter, *Philips Res. Rep.*, 1954, **9**, 295.
30 R. Shannon and C. T. Prewitt, *Acta Crystallogr. Sect. B*, 1969, **25**, 925.
31 H. P. Klug and L. E. Alexander, *X-Ray Diffraction Procedure for Polycrystalline and Amorphous Materials*, Wiley, New York, 2nd edn., 1974.
32 N. K. Gill and P. K. Puri, *Indian J. Pure Appl Phys.*, 1985, **23**, 71; V. A. M. Brabers and R. E. Vandenberghe, *Phys. Lett. A*, 1973, **44**, 493; P. Tarte and R. Collongues, *Ann. Chim.* (*Paris*), 1964, **9**, 135.
33 P. Tarte and J. Preudenhomme, *Spectrochim. Acta*, *Part A*, 1973, **29**, 1301.
34 P. Wartewig, K. Melzer, M. Krause and R. Tellgren, *J. Magn. Magn. Mater.*, 1995, **140**, 2101; S. Diaz, J. L. Sanchez, F. Leccabue, B. E. Watts, G. Bocelli and G. Albanese, *J. Phys. IV*, 1997, **7**, C1; P. M. Rao, A. Gerrad and F. Grandjean, *J. Magn. Magn. Mater.*, 1980, **15**, 645.
35 J. L. Dormann, *Rev. Phys. Appl.*, 1980, **15**, 1113.
36 J. L. Dormann, A. Tomas and M. Nogues, *Phys. Status Solidi A*, 1983, **77**, 611.
37 J. W. Young and J. Smit, *J. Appl. Phys.*, 1971, **42**, 2344.
38 S. K. Kulshreshtha and G. Ritter, *J. Mater. Sci.*, 1985, **20**, 821.

Paper 8/03939I